

## Differential Cross Sections of the $\text{Be}^9(\text{Li}^7, \alpha)\text{B}^{12}$ and $\text{Be}^9(\text{Li}^6, \alpha)\text{B}^{11}$ Reactions\*

RUSSELL K. HOBBIIE, C. W. LEWIS, AND J. M. BLAIR  
*School of Physics, University of Minnesota, Minneapolis, Minnesota*

(Received July 25, 1961)

Differential cross sections have been measured for  $\alpha$  particles from the reactions  $\text{Be}^9(\text{Li}^6, \alpha)\text{B}^{11}$  and  $\text{Be}^9(\text{Li}^7, \alpha)\text{B}^{12}$ . These reactions have been studied for the ground states, the first seven excited states of  $\text{B}^{11}$ , and the first four excited states of  $\text{B}^{12}$ . Absolute cross sections have been measured by comparison with Rutherford scattering. The measurements have been carried out for laboratory bombarding energies from 3.3 to 3.75 Mev.

### INTRODUCTION

THE reaction  $\text{Be}^9(\text{Li}^6, \alpha)\text{B}^{11}$  has previously been studied<sup>1</sup> in this laboratory using a proportional counter in combination with a CsI(Tl) scintillation counter to identify the alpha particles. Improvements in the energy resolution of the equipment have made it possible to extend these measurements to alpha particles leaving  $\text{B}^{11}$  in more highly excited states and to study the reaction  $\text{Be}^9(\text{Li}^7, \alpha)\text{B}^{12}$ , for which the ground-state  $Q$  value is 10.46 Mev. A separate study of the  $\text{Be}^9(\text{Li}^6, \alpha)\text{B}^{11}$  reaction, using a silicon junction detector alone to count the alpha particles, provided an independent check of the other measurements. In the work reported here the cross sections have been determined by comparing the reaction yields with Rutherford scattering from the same target at angles where nuclear perturbations of the scattering are small. This procedure is believed to provide more accurate values of the absolute cross sections than resulted from the previous work.

### APPARATUS

The equipment for producing the beam of Li ions, the target chamber, and the beam current integrator were unchanged from the earlier work.<sup>1</sup>

For the measurements made with the junction detector alone, hereafter referred to as method A, the detector was mounted on the movable portion of the target chamber with its sensitive surface at a distance of 4.2 cm from the target. The portion of the detector used for counting was defined by a circular aperture 0.185 cm in diameter which was located 0.1 cm in front of the surface of the detector. After suitable amplification, pulses from the detector were recorded by a 100-channel pulse-height analyzer.

Method B of detecting the alpha particles was a modification of the two-counter particle identification scheme used previously.<sup>1</sup> In the present work a silicon junction detector replaced the previous CsI(Tl) crystal as total energy counter, and an improved log-add circuit<sup>2</sup> combined the  $\Delta E$  and  $E$  pulses from the two

counters. Calculations and tests indicated that the combination ( $E^{0.6}\Delta E$ ) produced a particle identification signal which was nearly independent of the energy of the alpha particles and hence was suitable for gating the 100-channel pulse-height analyzer which recorded the spectrum of alpha-particle pulses from the silicon junction detector. Figure 1 illustrates a typical spectrum of alpha-particle pulses from the  $\text{Be}^9(\text{Li}^7, \alpha)\text{B}^{12}$  reaction as well as an 8.8-Mev  $\text{ThC}'$  calibration peak. Figure 2 shows a similar pulse spectrum from the  $\text{Be}^9(\text{Li}^6, \alpha)\text{B}^{11}$  reaction. The improved resolution in the present work can be seen by comparing Fig. 2 with Fig. 3 of reference 1.

### PROCEDURE

The preparation of the thin (60 to 100  $\mu\text{g}/\text{cm}^2$ ), self-supporting Be foils and the energy calibration of the electrostatic generator followed the procedure described earlier.<sup>1</sup>

In the application of method A for particle detection the alpha particle peaks in the spectrum of pulses were identified by using the linear relation between the pulse height and the particle energies calculated for each angle. The bias voltage on the silicon junction detector was adjusted so that its sensitive region would have sufficient thickness to stop completely the alpha particles being counted, while allowing protons, deuterons, and tritons produced by competing reactions to pass through without losing all of their energy. The bias potentials necessary varied from 3 to 15 v. At angles where bias adjustment did not remove the pulses produced by the singly charged particles from the region of the spectrum occupied by the alpha particle pulses, their relative positions were shifted by placing additional layers of Mylar film over the detector. In all cases this aperture was covered by one layer of quarter-mil Mylar which screened out the large number of Li ions elastically scattered from the target. If this were not done the pile-up of the many small pulses from these scattered ions would have reduced the resolution.

The procedure for method B was essentially the same as in the earlier work.<sup>1</sup>

Method A was used to study the  $\text{Be}^9(\text{Li}^6, \alpha)\text{B}^{11}$  reaction at bombarding energies of 3.30 and 3.75 Mev, while method B was used at 3.3 Mev for the reaction  $\text{Be}^9(\text{Li}^6, \alpha)\text{B}^{11}$  and at 3.30, 3.50, and 3.75 Mev for the  $\text{Be}^9(\text{Li}^7, \alpha)\text{B}^{12}$  reaction. Measurements were made at

\* This work was supported in part by the joint program of the U. S. Atomic Energy Commission and the Office of Naval Research.

<sup>1</sup> J. J. Leigh and J. M. Blair, *Phys. Rev.* **121**, 246 (1961).

<sup>2</sup> G. Gianelli and L. Stanchi, *Nuclear Instr. and Methods* **8**, 79 (1960).

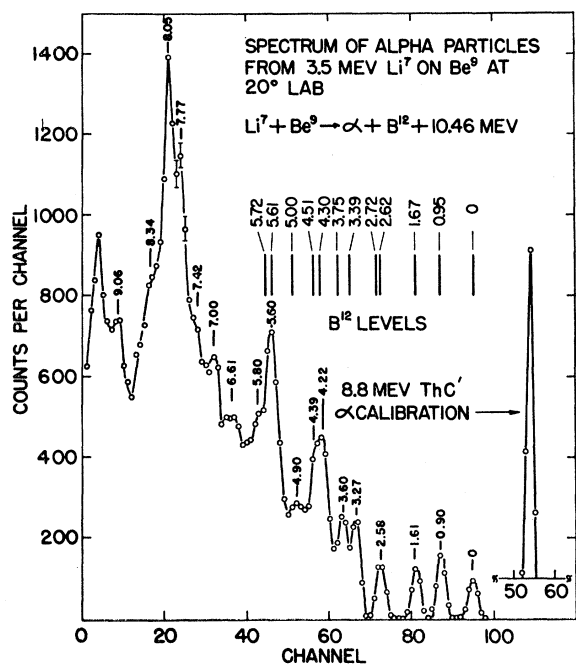


FIG. 1. Typical  $\alpha$ -particle spectrum from the reaction  $\text{Be}^9(\text{Li}^7, \alpha)\text{B}^{12}$ .

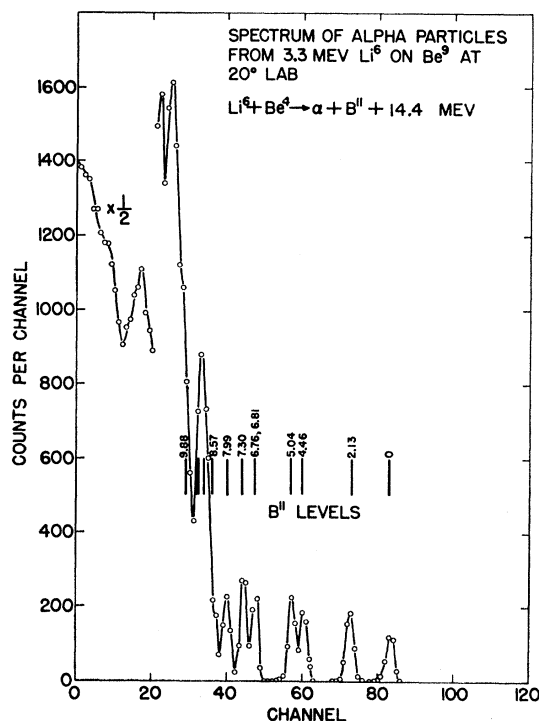


FIG. 2. Typical  $\alpha$ -particle spectrum from the reaction  $\text{Be}^9(\text{Li}^6, \alpha)\text{B}^{11}$ .

$10^\circ$  intervals from  $20^\circ$  to  $160^\circ$  in the laboratory, with some additional observations at  $10^\circ$ . Due to the deterioration of the targets and the buildup of surface contamination after long bombardment, several target foils were used. The data from these targets were normalized by repeating the measurements on a single target at a few angles at all the energies and then measuring the thickness of this target by the scattering technique described below.

#### DETERMINATION OF THE ABSOLUTE CROSS SECTION

In the earlier work, the absolute values of the cross sections were calculated from the target thickness measured by observing the increase in bombarding energy required to excite the  $\text{H}^1(\text{Li}^7, \gamma)\text{Be}^8$  reaction, when the Be foil was placed in the  $\text{Li}^7$  beam in front of an ice target.<sup>1</sup> The good resolution of the silicon junction detectors made it possible to measure the target thickness by Rutherford scattering, and some errors in the earlier method were discovered.

If the solid angle is the same for the Rutherford scattering and the nuclear reaction, the cross section for the nuclear reaction may be found without measuring the target thickness or the solid angle. The nuclear laboratory cross section,  $\sigma_N$ , is given in terms of the laboratory Rutherford cross section,  $\sigma_R$ , by the following equation:

$$\sigma_N(\theta, E) = \frac{Y_N(\theta, E)\sigma_R(\theta', E')Q_R\bar{z}(E)}{Y_R(\theta', E')Q_N\bar{z}(E')}$$

where  $Y_N$  = number of nuclear events recorded during the collection of charge  $Q_N$  by the Faraday cup,  $Y_R$  = number of Rutherford events observed during the collection of charge  $Q_R$  by the Faraday cup, and  $\bar{z}(E)$  = equilibrium charge of the Li beam after passing through the target.

When using method A, the scattered  $\text{Li}^6$  ions were counted by removing the layer of Mylar from the front of the silicon junction detector. For method B, the Mylar window of the proportional counter was removed and the amplified pulses from the junction detector were displayed on the pulse-height analyzer without using the multiplying and gating circuit. The Rutherford scattering was measured at an energy  $E' = 3.3$  Mev, at laboratory angles from  $30^\circ$  to  $50^\circ$ . At smaller angles it was impossible to separate the lithium ions scattered from carbon and oxygen contaminants on the targets; at larger angles the energy of the ions was too small for detection. For the angles studied the apsidal distance of the Rutherford orbit was greater than  $20f$ , and the nuclear perturbation should be negligible. This was confirmed by the constancy of the ratio  $Y_R(\theta)/\sigma_R(\theta)$  with angle. Previous measurements<sup>1</sup> indicate that  $\bar{z}$  varies by no more than 2% over the range of energies used in this experiment.

The pulse-height spectrum of Li ions scattered from a typical target is displayed in Fig. 3. Li groups scattered from Be, C, and O are seen along with recoil target nuclei. This particular target had severe use,

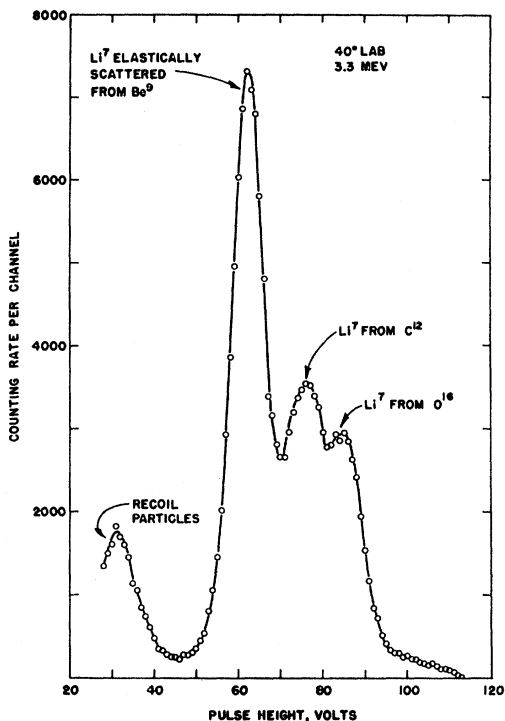


FIG. 3. Typical spectrum of scattered particles when  $\text{Li}^7$  undergoes Rutherford scattering from a  $\text{Be}^9$  target.

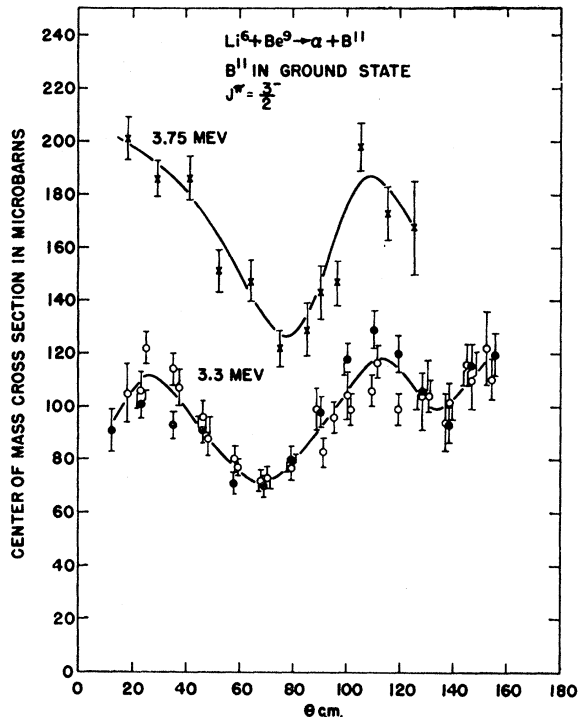


FIG. 5. Differential cross section for  $\alpha$  particles from  $\text{Be}^9(\text{Li}^6, \alpha)\text{B}^{11}$ , leaving  $\text{B}^{11}$  in the ground state. Crosses and open circles represent data taken by method A; solid dots were taken by method B.

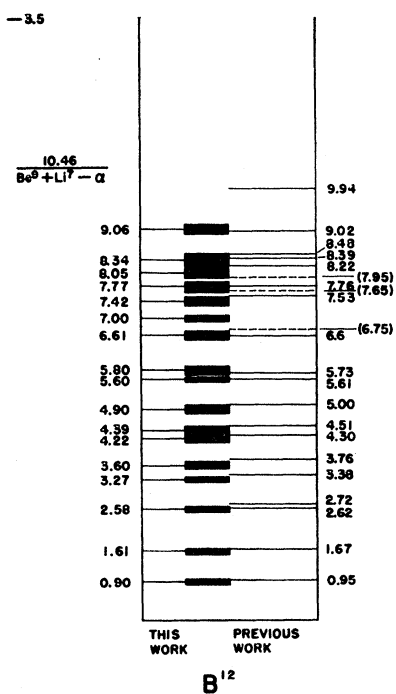


FIG. 4. Energy levels in  $\text{B}^{12}$ . Values from this work are given on the left; the sources of values on the right are discussed in the text.

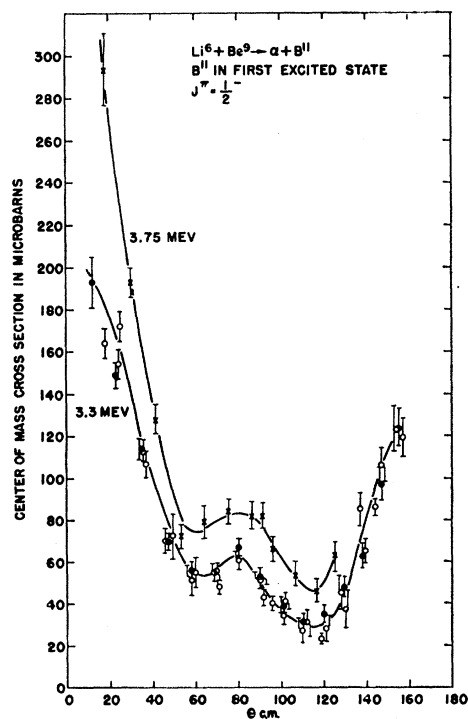


FIG. 6. Differential cross section for  $\alpha$  particles from  $\text{Be}^9(\text{Li}^6, \alpha)\text{B}^{11}$ , leaving  $\text{B}^{11}$  in the first excited state. Crosses and open circles represent data taken by method A; solid dots were taken by method B.

and the continual breakdown of diffusion pump oil by the beam resulted in a relatively large deposit of carbon on the target. The combined thickness of Be, C, and O calculated from these scattering data agrees well with the total thickness measured by the energy loss method. When the earlier measurements<sup>1</sup> were made, the degree of buildup of target contaminants was not appreciated; hence the cross sections were calculated using too large a number for the target thickness. Therefore, the corrected values of the cross sections given in this paper should be used rather than those in reference 1.

### RESULTS

Typical alpha-particle pulse-height spectra obtained by method B are shown in Figs. 1 and 2 for the  $\text{Be}^9(\text{Li}^7, \alpha)\text{B}^{12}$  and the  $\text{Be}^9(\text{Li}^6, \alpha)\text{B}^{11}$  reactions, respectively. Vertical lines indicate the peak positions calculated from the tabulated<sup>8</sup> energy levels and corrected for energy loss in the proportional counter and the response characteristic of the junction detector. The low-energy continuum with the  $\text{Li}^6$  beam is thought to be due to  $\alpha$  particles from the reaction  $\text{Be}^9(\text{Li}^6, \text{Li}^7)\text{Be}^8$ , while the continuum with the  $\text{Li}^7$  beam can be explained in terms of the reaction  $\text{Be}^9(\text{Li}^7, \text{He}^5)\text{B}^{11}$ .

The peaks in Fig. 1 are labeled with the corresponding  $\text{B}^{12}$  excitation energies. The lowest energy peak has

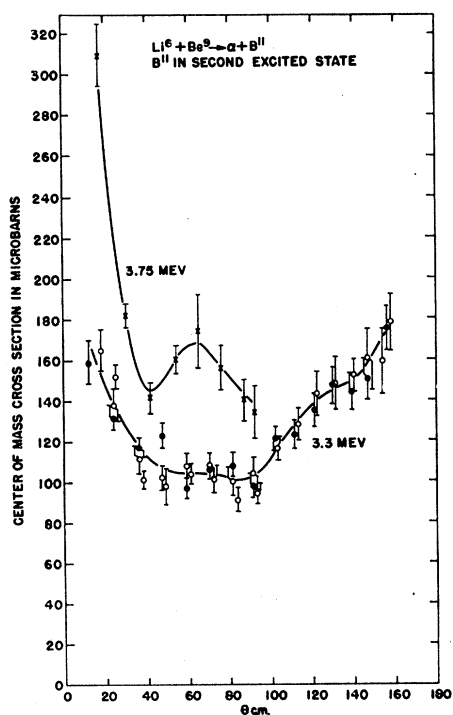


FIG. 7. Differential cross section for  $\alpha$  particles from  $\text{Be}^9(\text{Li}^6, \alpha)\text{B}^{11}$ , leaving  $\text{B}^{11}$  in the second excited state. Crosses and open circles represent data taken by method A; solid dots were taken by method B.

<sup>3</sup> F. Ajzenberg-Selove and T. Lauritsen, Landolt-Börnstein Tables (to be published).

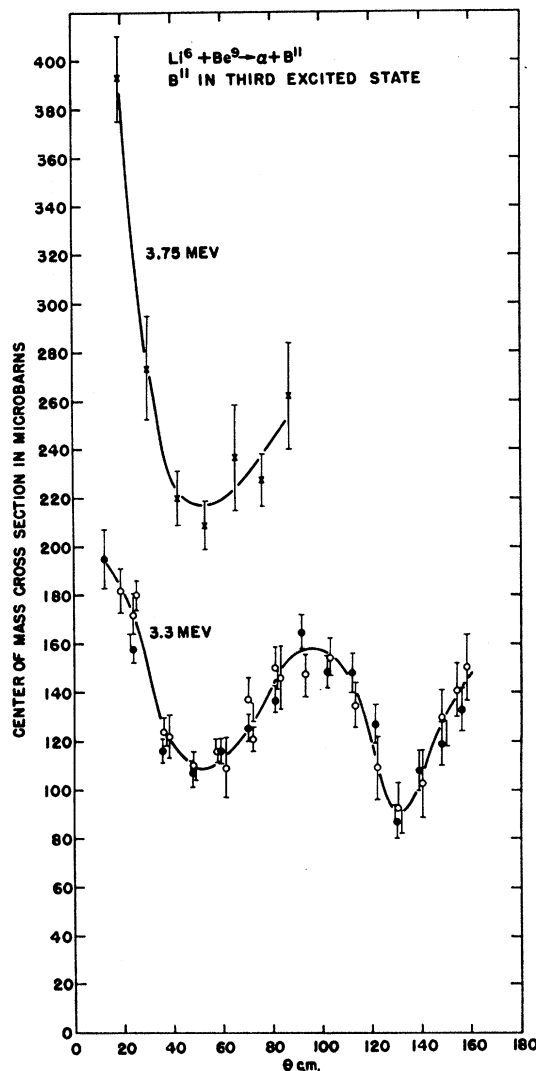


FIG. 8. Differential cross section for  $\alpha$  particles from  $\text{Be}^9(\text{Li}^6, \alpha)\text{B}^{11}$ , leaving  $\text{B}^{11}$  in the third excited state. Crosses and open circles represent data taken by method A; solid dots were taken by method B.

been neglected because it could not be observed at any other angles. These results are also shown in Fig. 4. The numbers on the left are calculated from the present data; the heavy bars indicate the uncertainty in the calculated value. The levels below 6.0 Mev on the right are from the compilation of levels<sup>3</sup>; the levels above 6.0 Mev are from measurements<sup>4</sup> of the total neutron cross section of boron.

Center-of-mass differential cross sections are plotted in Figs. 5-11 for  $\text{Be}^9(\text{Li}^6, \alpha)\text{B}^{11}$  and Figs. 12-15 for  $\text{Be}^9(\text{Li}^7, \alpha)\text{B}^{12}$ . It was not possible to resolve the third and fourth levels of  $\text{B}^{11}$ , so the combined cross sections are plotted. Cross sections for more highly excited states

<sup>4</sup> D. B. Fossan, *et al.*, Phys. Rev. **123**, 209 (1961).

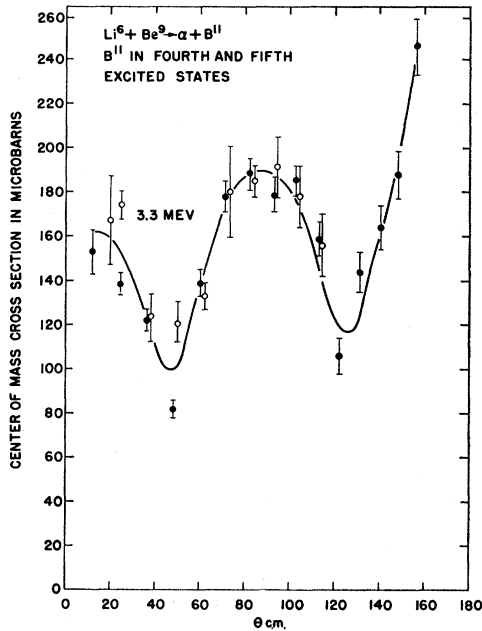


FIG. 9. Differential cross section for  $\alpha$  particles from  $\text{Be}^9(\text{Li}^6, \alpha)\text{B}^{11}$ , leaving  $\text{B}^{11}$  in the fourth and fifth excited states. Open circles represent data taken by method A; solid dots were taken by method B.

could not be extracted because of the  $\alpha$ -particle continuum backgrounds mentioned above.

Error bars represent the standard deviation due to counting statistics except for a few points measured by method A, for which the error bars have been increased

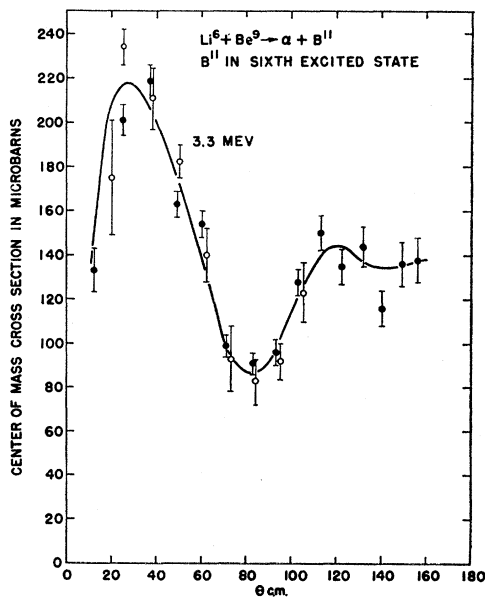


FIG. 10. Differential cross section for  $\alpha$  particles from  $\text{Be}^9(\text{Li}^6, \alpha)\text{B}^{11}$ , leaving  $\text{B}^{11}$  in the sixth excited state. Open circles represent data taken by method A; solid dots were taken by method B.

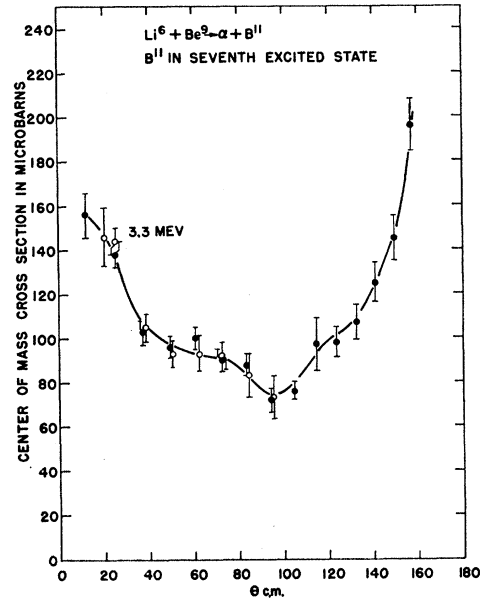


FIG. 11. Differential cross section for  $\alpha$  particles from  $\text{Be}^9(\text{Li}^6, \alpha)\text{B}^{11}$ , leaving  $\text{B}^{11}$  in the seventh excited state. Open circles represent data taken by method A; solid dots were taken by method B.

because of uncertainty in subtracting a proton background from the peak. The absolute cross section scales have an additional uncertainty of 10%, due mainly to uncertainty in estimating the number of counts under the  $\text{Li}^7\text{-Be}^9$  elastic scattering peak. All cross sections be increased by 9% to correct for the energy loss in the target.

The differential cross sections were integrated numerically to give the total cross sections presented in

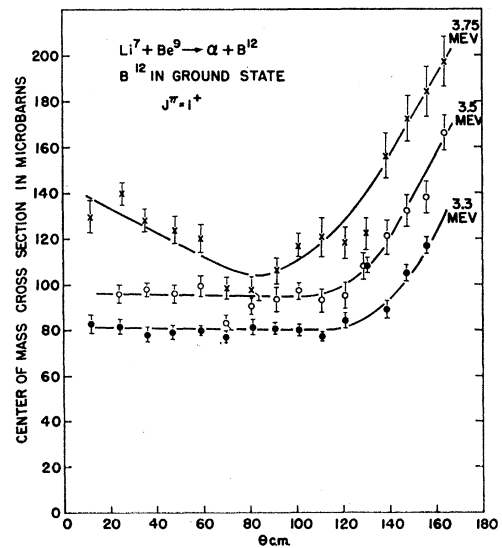


FIG. 12. Differential cross section for  $\alpha$  particles from  $\text{Be}^9(\text{Li}^7, \alpha)\text{B}^{12}$ , leaving  $\text{B}^{12}$  in the ground state.

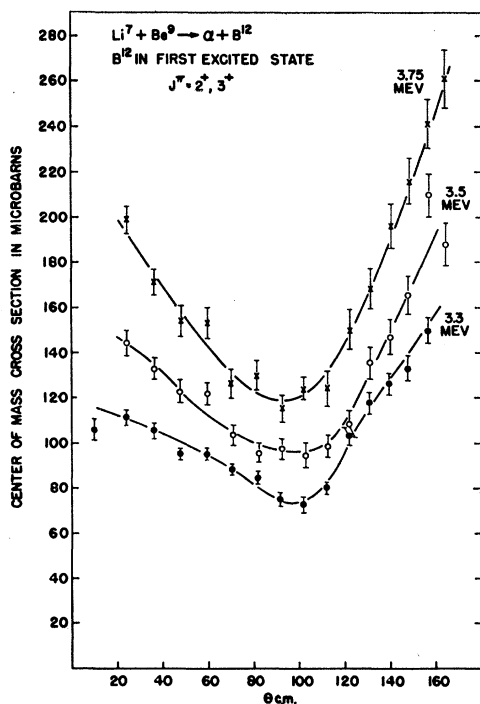


FIG. 13. Differential cross section for  $\alpha$  particles from  $\text{Be}^9(\text{Li}^7, \alpha)\text{B}^{12}$ , leaving  $\text{B}^{12}$  in the first excited state.

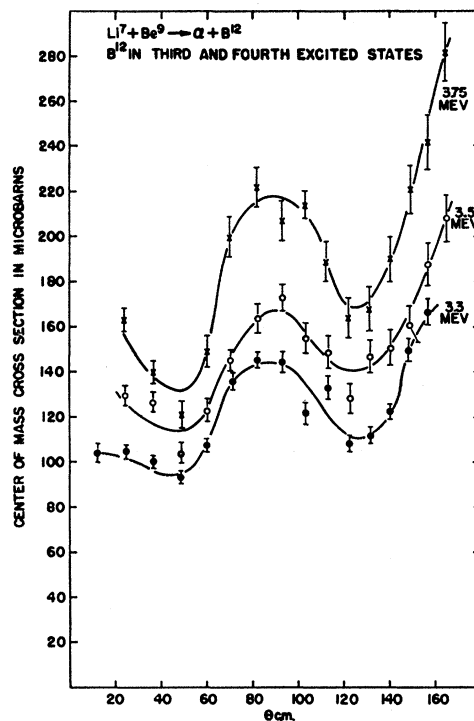


FIG. 15. Differential cross section for  $\alpha$  particles from  $\text{Be}^9(\text{Li}^7, \alpha)\text{B}^{12}$ , leaving  $\text{B}^{12}$  in the third and fourth excited states.

Table I. Absolute errors are again 10%, although the relative yields for various levels of the same reaction are accurate to 2%.

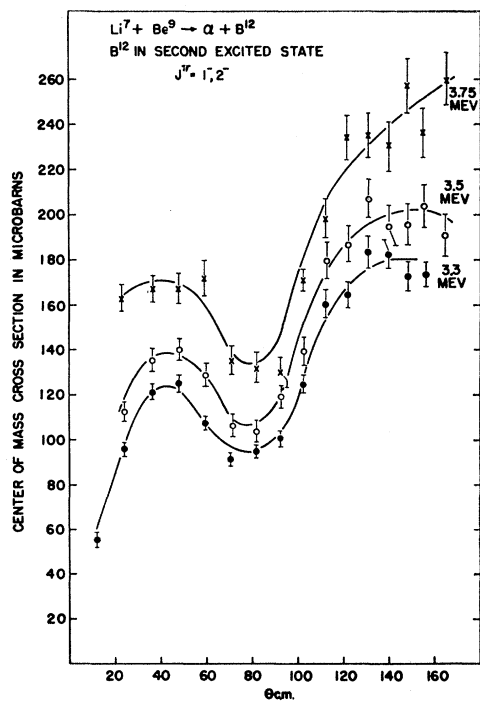


FIG. 14. Differential cross section for  $\alpha$  particles from  $\text{Be}^9(\text{Li}^7, \alpha)\text{B}^{12}$ , leaving  $\text{B}^{12}$  in the second excited state.

DISCUSSION

The angular distributions for the reaction  $\text{Be}^9(\text{Li}^6, \alpha)\text{B}^{11}$  are in good agreement by the two methods and also agree with the earlier measurements by Leigh and Blair.<sup>1</sup> The absolute cross sections represent a correction of the earlier work because the degree of target contamination was not appreciated at that time. Although the increase in yield between 3.3 and 3.75 Mev seems large for the third excited state compared to the first excited state, these data are consistent with the results presented in Fig. 9 of reference 1.

The data for  $\text{Be}^9(\text{Li}^7, \alpha)\text{B}^{12}$  suggest that the group corresponding to levels 3 and 4 in  $\text{B}^{12}$  is due to excitation of the 2.62-Mev level, although the resolution is not sufficient to rule out an equal mixture of the two levels.

TABLE I. Total cross section in millibarns for  $\text{Be}^9(\text{Li}^6, \alpha)\text{B}^{11}$  and  $\text{Be}^9(\text{Li}^7, \alpha)\text{B}^{12}$  at three laboratory bombarding energies.

Target	Excited state	3.3 Mev	3.5 Mev	3.75 Mev
$\text{B}^{11}$	0	1.25		
	1	0.85		
	2	1.54		
	3	1.65		
	4,5	2.00		
	6	1.70		
	7	1.29		
	$\text{B}^{12}$	0	1.07	1.27
	1	1.24	1.51	1.94
	2	1.62	1.84	2.25
	3,4	1.56	1.83	2.32

Measurements with a magnetic spectrometer<sup>5</sup> of the reaction  $B^{11}(d,p)B^{12}$  showed that the cross section for the 2.72-Mev level was 5% of the cross section for the 2.62-Mev state. Recent measurements<sup>6</sup> of protons from  $B^{10}(t,p)B^{12}$  confirm that the 2.72-Mev state is weakly excited. With a different mode of excitation one cannot rule out the possibility of a greater population of the 2.72-Mev level; however, the total cross section for this group of  $\alpha$  particles is not significantly larger than for the groups corresponding to single levels.

The 7.0-Mev level which we observe in  $B^{12}$  is unambiguously present, and our 8.05-Mev level is quite

<sup>5</sup> M. M. Elkind, Phys. Rev. **92**, 127 (1953).

<sup>6</sup> A. A. Jaffe, *et. al.*, Proc. Phys. Soc. (London) **A76**, 914 (1960)

strongly excited. Neither of these levels was observed in the total neutron cross-section measurements<sup>4</sup> on  $B^{11}$ . If these levels were due to target contaminants we should have observed additional sharp  $\alpha$ -particle peaks of higher energy due to these same contaminants. There are several reasons<sup>4</sup> why peaks might not have been seen in the neutron work; e.g., the  $B^{12}$  level could have  $J=0$ .

#### ACKNOWLEDGMENTS

The authors are grateful to Fred Forbes, Earl Knutson, Lawrence Pinnsonault, and Dr. J. J. Leigh for their help in operating the Van de Graaf generator and taking data. Alan Linhoff assisted in the data reduction.

## Angular Distribution of Alpha Particles Emitted by Oriented $Np^{237}$ Nuclei

S. H. HANAUER, J. W. T. DABBS, L. D. ROBERTS, AND G. W. PARKER  
Oak Ridge National Laboratory,\* Oak Ridge, Tennessee

(Received June 28, 1961)

$Np^{237}$  nuclei were aligned through the electric quadrupole and magnetic hyperfine couplings in  $NpO_2Rb(NO_3)_3$ , cooled to 0.2–4.2°K. A complete experiment, with rotatable monocrystalline sample, solid-state counter, thermometer, and goniometer, was enclosed in a copper container filled with  $He^3$  gas and thermally attached to  $\frac{1}{2}$  mole of paramagnetic salt which could be cooled magnetically. The measured temperature dependence of the  $\alpha$ -particle anisotropy gives  $A < 0$ ,  $P > 0$  for the signs of the hyperfine coupling constants in  $NpO_2^{++}$ . The  $\alpha$  particles were observed to be emitted preferentially along the direction of the nuclear angular momentum vector. The results are consistent with  $P-\pi$  bonding in the  $NpO_2^{++}$  ion and with Hill and Wheeler's prediction of the role of barrier penetration in  $\alpha$  emission from nonspherical nuclei.

### I. INTRODUCTION

ALPHA-PARTICLE emission from oriented nuclei was first considered by Spiers.<sup>1</sup> In a formal way, he pointed out that if there were angular momentum changes in the alpha emission process, a spatial anisotropy of emission would in general be expected when the parent nuclei were oriented. No specific nuclear model was considered in this work, however, and no detailed prediction of the character of this anisotropy was given.

A general theory of angular momentum effects in alpha emission has been given by Rose<sup>2</sup> in which the angular distribution of the alpha particles is completely specified in terms of nuclear matrix elements.

It was suggested by Hill and Wheeler<sup>3</sup> that a nonspherical shape for an alpha-emitting nucleus should have an effect upon the angular distribution of the alpha particles emitted. For example, they found that for a nucleus of prolate spheroidal shape the potential barrier against alpha-particle emission should be both lower and thinner near the nuclear "poles" than near the nuclear

"equator." Assuming a uniform probability of alpha-particle formation over the nuclear surface, they pointed out that a strong preferential alpha emission near the nuclear "poles" would be expected. Using a simplified WKB treatment they estimated this preferential emission to be sixteen times more intense at the polar than at the equatorial region for a moderate spheroidal deformation of the nucleus of  $c/a \approx 1.1$ . They further suggested that these effects could be investigated by nuclear orientation experiments, but angular momentum effects were not included in their discussion. Barrier effects in alpha emission have also been studied by Christy,<sup>4</sup> whose conclusions are in general accord with those of Hill and Wheeler.

Recently, more complete theoretical discussions of alpha emission including angular momentum effects and considering specific nuclear models have been given, for example, by Brussaard and Tolhoek,<sup>5</sup> Rasmussen and Segall,<sup>6</sup> Steenberg and Sharma,<sup>7</sup> and Fröman.<sup>8</sup> It is

\* Operated by Union Carbide Corporation for the U. S. Atomic Energy Commission.

<sup>1</sup> J. A. Spiers, Nature **161**, 807 (1948).

<sup>2</sup> M. E. Rose, *Elementary Theory of Angular Momentum* (John Wiley & Sons, Inc., New York, 1957), pp. 176–186.

<sup>3</sup> D. L. Hill and J. A. Wheeler, Phys. Rev. **89**, 1133 (1953).

<sup>4</sup> R. F. Christy, Bull. Am. Phys. Soc. **30**, 66 (1955).

<sup>5</sup> P. J. Brussaard and H. A. Tolhoek, Physica **24**, 233 (1958).

<sup>6</sup> J. O. Rasmussen and B. Segall, Phys. Rev. **103**, 1298 (1956).

<sup>7</sup> N. R. Steenberg and R. C. Sharma, Can. J. Phys. **38**, 290 (1960).

<sup>8</sup> P. O. Fröman, Kgl. Danske Videnskab. Selskab, Mat.-fys. Skrifter **1**, No. 3 (1957).